Research Square

Preprints are preliminary reports that have not undergone peer review.
They should not be considered conclusive, used to inform clinical practice,
or referenced by the media as validated information.

Oncogenic 3D genome conformations identify novel therapeutic targets in ependymoma

Konstantin Okonechnikov
Hopp Children's Cancer Center (KiTZ)
Aylin Camgoz
Hopp Children's Cancer Center (KiTZ)
Donglim Esther Park
UCSD
Owen Chapman
UCSD
Jens-Martin Hübner
Hopp Children's Cancer Center (KiTZ)
Abhijit Chakraborty
La Jolla Institute for Immunology
Meghana Pagadala
UCSD
Rosalind Bump
Salk Institute for Biological Studies
Sahaana Chandran
Salk Institute for Biological Studies
Katerina Kraft
Stanford University
Rocio Acuna-Hidalgo
10. Max Planck Institute for Molecular Genetics
Derek Reid
Arima Genomics, Inc
Edwin F. Juarez
UCSD
James T. Robinson
UCSD
Kristian W. Pajtler
German Cancer Research Center
Monika Mauermann
Hopp Children's Cancer Center NCT Heidelberg (KiTZ)
Till Milde

German Cancer Research Center (DKFZ) https://orcid.org/0000-0002-7267-1052

Nicole G. Coufal
UCSD

Michael Levy
Rady Children's Hospital-San Diego

Denise Malicki
Rady Children's Hospital

Shareef Nahas
Rady Children's Hospital

Matija Snuderl
NYU Langone Health

John Crawford
Rady Children's Hospital

Robert J. Wechsler-Reya
Sanford Burnham Prebys Medical Discovery Institute https://orcid.org/0000-0002-7463-8352

Stefan Mundlos
Max Planck Institute for Molecular Genetics https://orcid.org/0000-0002-9788-3166

Anthony Schmitt
Arima Genomics

Hannah Carter
UCSD

Kulandaimanuvel Antony Michaelraj
Hospital for Sick Children

Sachin A. Kumar
The Hospital for Sick Children https://orcid.org/0000-0002-4853-3864

Michael D. Taylor
Sickkids Hospital

Jeremy Rich
Division of Regenerative Medicine, Department of Medicine, University of California San Diego

Frank Buchholz
TU Dresden

Jill P. Mesirov
University of California, San Diego

Stefan M. Pfister
Division of Pediatric Neurooncology, German Cancer Research Center (DKFZ)

Ferhat Ay
La Jolla Institute For Immunology https://orcid.org/0000-0002-0708-6914

Jesse R. Dixon
Salk Institute for Biological Studies https://orcid.org/0000-0002-6273-2181

Marcel Kool
Division of Pediatric Neuro-oncology and German Cancer Consortium (DKTK), German Cancer Research Center (DKFZ), Heidelberg
Lukas Chavez (lukaschavez@health.ucsd.edu)
University of California, San Diego

Biological Sciences - Article

Keywords: ependymoma, tumorigenesis, oncogenic mechanisms

Posted Date: November 5th, 2020

DOI: https://doi.org/10.21203/rs.3.rs-88331/v1

License: This work is licensed under a Creative Commons Attribution 4.0 International License.
Read Full License

Oncogenic 3D genome conformations identify novel therapeutic targets in ependymoma.

Konstantin Okonechnikov[1,2,*], Aylin Camgoz[1,2,3,*], Donglim Esther Park[4,5], Owen Chapman[6], Jens-Martin Hübner[1,2], Abhijit Chakraborty[7], Meghana Pagadala[6], Rosalind Bump[8], Sahaana Chandran[8], Katerina Kraft[9], Rocio Acuna-Hidalgo[10,11], Derek Reid[12], Edwin F. Juarez[6], James T. Robinson[6], Kristian W. Pajtler[1,2,13], Monika Mauermann[1,2], Till Milde[1,13,14], Nicole G. Coufal[15,18], Michael Levy[16], Denise Malicki[17], Shareef Nahas[18], Matija Snuderl[19,20], John Crawford[21], Robert J. Wechsler-Reya[5,14,22], Stefan Mundlos[10], Anthony Schmitt[12], Hannah Carter[6], Kulandaimanuvel Antony Michealraj[23], Sachin A. Kumar[23], Michael D. Taylor[23], Jeremy Rich[4,5,24], Frank Buchholz[3,25,26], Jill P. Mesirov[6,27], Stefan M. Pfister[1,2,13], Ferhat Ay[7,14], Jesse R. Dixon[8], Marcel Kool[1,2,28,#], Lukas Chavez[6,27,#,+]

1. Hopp Children's Cancer Center (KiTZ), Heidelberg, Germany;
2. Division of Pediatric Neurooncology, German Cancer Research Center (DKFZ) and German Cancer Consortium (DKTK), Heidelberg, Germany;
3. National Center for Tumor Diseases (NCT): German Cancer Research Center (DKFZ) Heidelberg, Faculty of Medicine and University Hospital Carl Gustav Carus, Technische Universität Dresden, Helmholtz-Zentrum Dresden-Rossendorf (HZDR), Dresden, Germany;
4. Division of Regenerative Medicine, Department of Medicine, University of California, San Diego, La Jolla, CA 92037, USA;
5. Sanford Consortium for Regenerative Medicine, 2880 Torrey Pines Scenic Drive, La Jolla, CA 92037, USA;
6. Division of Medical Genetics, Department of Medicine, University of California San Diego (UCSD), San Diego, USA;
7. Centers for Cancer Immunotherapy and Autoimmunity, La Jolla Institute for Immunology, La Jolla, CA, USA;
8. Peptide Biology Labs, Salk Institute for Biological Studies, La Jolla, CA, USA;
9. Center for Personal Dynamic Regulomes, Stanford University, Stanford, CA, USA ;
10. Max Planck Institute for Molecular Genetics, Berlin, Germany;
11. Institute for Medical Genetics and Human Genetics, Charité Universitätsmedizin Berlin, Berlin, Germany;
12. Arima Genomics, Inc. San Diego, CA, 92121;

13. Department of Pediatric Oncology, Hematology and Immunology, Heidelberg University Hospital, Heidelberg, Germany;
14. CCU Pediatric Oncology, German Cancer Research Center (DKFZ) and German Cancer Consortium (DKTK), Heidelberg, Germany;
15. Department of Pediatrics, University of California, San Diego, San Diego, CA 92093, USA;
16. Neurosurgery, University of California San Diego – Rady Children's Hospital, San Diego, CA 92123, USA;
17. Pathology, University of California San Diego – Rady Children's Hospital, San Diego, CA 92123, USA;
18. Rady Children's Institute for Genomic Medicine, San Diego, California 92123, USA;
19. Department of Pathology, NYU Langone Health, NYU Grossman School of Medicine, 550 First Ave, New York, NY 10016 USA;
20. Laura and Isaac Perlmutter Cancer Center, NYU Langone Health, New York, NY USA;
21. Department of Neurosciences, University of California San Diego – Rady Children's Hospital, San Diego, CA 92123, USA;
22. Tumor Initiation and Maintenance Program, NCI-Designated Cancer Center, Sanford Burnham Prebys Medical Discovery Institute, La Jolla, CA, USA;
23. Division of Neurosurgery, Arthur and Sonia Labatt Brain Tumor Research Center, Hospital for Sick Children, University of Toronto, Toronto, Ontario, Canada;
24. Department of Neurosciences, School of Medicine, University of California San Diego, La Jolla, CA 92037, USA;
25. Medical Systems Biology, Medical Faculty and University Hospital Carl Gustav Carus, TU Dresden, 01307 Dresden, Germany;
26. German Cancer Research Center (DKFZ), Heidelberg and German Cancer Consortium (DKTK) Partner Site Dresden, Germany;
27. Moores Cancer Center, University of California San Diego (UCSD), La Jolla, CA, USA;
28. Princess Máxima Center for Pediatric Oncology, Utrecht, The Netherlands.

*These authors contributed equally to this work.

#These authors are co-senior authors.

+ Manuscript correspondence.

Abstract

Ependymoma is a tumor of the brain or spinal cord. The two most common and aggressive molecular groups of ependymoma are the supratentorial RELA-fusion associated group and the posterior fossa ependymoma group A. In both groups, tumors occur mainly in young children and frequently recur after treatment[1]. Although the molecular mechanisms underlying these diseases have recently been uncovered, they remain difficult to target and innovative therapeutic approaches are urgently needed. Here, we use genome-wide chromosome conformation capture (Hi-C), complemented with CTCF (insulators) and H3K27ac (active enhancers) ChIP-seq as well as gene expression and whole-genome DNA methylation profiling in primary and relapsed ependymoma tumors and cell lines to identify chromosomal rearrangements and regulatory mechanisms underlying aberrant expression of genes that are essential for ependymoma tumorigenesis. In particular, we observe the formation of new topologically associating domains ('neo-TADs') by intra- and inter-chromosomal structural variants, tumor-specific 3D chromatin complexes of regulatory elements, and the replacement of CTCF insulators by DNA hyper-methylation as novel oncogenic mechanisms in ependymoma. Through inhibition experiments we validated that the newly identified genes, including *RCOR2*, *ITGA6*, *LAMC1*, and *ARL4C*, are highly essential for the survival of patient-derived ependymoma models in a disease subtype-specific manner. Thus, this study identifies potential novel therapeutic vulnerabilities in ependymoma and extends our ability to reveal tumor-dependency genes and pathways by oncogenic 3D genome conformations even in tumors that lack known genetic alterations.

Main

Tumors of the central-nervous system (CNS) are the most common cancers in children aged 0-14 years and a leading cause of death during childhood[2-4]. Intracranial ependymomas are segregated on the basis of anatomical location (supratentorial versus infratentorial or posterior fossa) and further divided by DNA methylation and expression profiling into distinct molecular groups that reflect differences in the age of onset, gender predominance, response to therapy, and genetic aberrations that drive the disease[1,5,6]. The supratentorial RELA-fusion associated group is characterized by recurrent complex chromothripsis events in chromosome 11 that lead to different types of *C11orf95-RELA* fusion genes, which have been shown to drive tumorigenesis in this group of tumors[7,8]. In contrast, initial DNA sequencing studies showed an absence of recurrent mutations or gene fusions in posterior fossa ependymoma group A (PFA), suggesting that these tumors might be epigenetically driven[5,7]. Indeed, global loss of histone H3 lysine 27 trimethylation (H3K27me3), a histone modification associated with the negative regulation of gene expression, was identified as a marker for PFA tumors[9]. Recent studies

have revealed that EZH inhibitory protein EZHIP (previously known as *CXorf67*), which is aberrantly expressed in most PFA ependymomas, causes downregulation of H3K27me3 by inhibiting EZH2 in the polycomb repressive complex 2 (PRC2)[10,11]. The few PFA ependymomas that do not overexpress *EZHIP* appeared to harbor K27M mutations in H3.1 or H3.3, which also inhibit EZH2. Furthermore, gain of chromosome arm 1q, present in ~25% of all PFA tumors, has been associated with a particularly poor survival of PFA patients, but the underlying driver mechanism remains unknown[10,12]. Since there are no small molecules available directly targeting the C11orf95-RELA fusions or EZHIP, and since it is not yet known whether EZHIP alone drives tumorigenesis in PFA, a better understanding of the tumor driving mechanisms and how they can be targeted is urgently needed. New insights into the regulation of gene expression during normal and diseased human development have recently been gained by analyzing 3D chromatin architectures[13-15]. Therefore, we have combined Hi-C with complementary molecular profiling techniques of ependymoma tumors and cell lines to investigate whether changes in intra- or inter- chromosomal DNA interactions in these tumors may lead to activation of specific oncogenes and may identify novel targets and tumor dependencies (**Figure 1a**).

The 3D genome organization of ependymoma tumors

We have performed Hi-C[16] followed by deep sequencing in 14 PFA and RELA ependymoma samples, comprising eleven tumors (fresh frozen or FFPE) and three cell lines (**Figure 1b, Suppl. Figure 1a**). Most samples were also analyzed by chromatin immunoprecipitation targeting the histone modification H3K27ac, which is associated with active chromatin, followed by sequencing (ChIP-seq, n=9), gene expression (RNA-seq, n=11), whole genome sequencing (WGS, n=12) and DNA methylation (n=14, **Suppl. Table 1**). PFA and RELA ependymoma groups can be clearly distinguished using various molecular profiling techniques including DNA methylation[17] (**Suppl. Figure 1b**). Unsupervised clustering of the Hi-C data also clusters ependymoma tumors into the expected groups, demonstrating pronounced group-specific 3D tumor genome conformations (**Figure 1c, Suppl. Figure 1c,d**). By an integrative analysis of the Hi-C data, enhancers (defined by H3K27ac ChIP-seq enrichments), and gene expression, we observed that genes are generally expressed at higher levels when their promoters physically interact with enhancers or other gene promoters (**Figure 1d**). A large percentage (~63-66%) of enhancer-associated genes (EAGs) previously predicted to be regulated by PFA or RELA enhancers[18] can be confirmed to have chromatin interactions between gene promoters and enhancers by the analysis of subgroup-specific Hi-C maps (**Figure 1e**). For example, the *Tenascin C* (*TNC*) promoter physically interacts with distal PFA enhancers (**Figure 1f**), which are positively correlated with *TNC* expression across a cohort of 24 tumors from six different intracranial ependymoma groups (**Figure 1g, Suppl. Figure 1e**). Overall, we found that more than twice as many

genes as previously reported[18] are potentially regulated by proximal and distal ependymoma enhancers (**Figure 1h, Suppl. Table 2,3**). For example, the gene encoding Eukaryotic Translation Elongation Factor 1 Alpha 2 (*EEF1A2*) interacts with subgroup specific enhancers (**Figure 1i)** and is specifically upregulated in RELA -fusion associated tumors (**Figure 1j**). These and other regulatory dependencies were not recognized in our previous study[18], due to lack of data on chromatin interactions in ependymoma samples and because TAD annotations from a fetal lung fibroblast cell line (IMR90) were used instead (**Suppl. Figure 1f,g**).

Transcriptional activation of RCOR2 by neo-TAD formation in supratentorial RELA ependymoma

The formation of new topologically associating domains ('neo-TADs') through structural variation was recently shown to have a critical role in gene dysregulation and oncogenesis[19,20]. To dissect the effect of structural variants (SVs) in supratentorial RELA tumors on the potential formation of neo-TADs, we used newly developed computational tools for the detection of SVs based on Hi-C data[19,21] (**Suppl. Table 4**). We first took a closer look at the *C11orf95* and *RELA* gene loci, because it was previously shown that the oncogenic *C11orf95-RELA* gene fusions are a result of chromothriptic events on chromosome 11. As expected, the Hi-C data reproducibly detected structural variants at the *C11orf95* and *RELA* gene loci in the supratentorial RELA but not in PFA tumors (**Figure 2a, Suppl. Figure 2a**). Furthermore, the Hi-C data captured extraordinarily complex rearrangements within chromosome 11 in some RELA ependymoma samples (**Figure 2b**) and revealed that SVs are not restricted to chromosome 11 but also include inter-chromosomal rearrangements (**Figure 2c**). In particular, we observed intra- and inter-chromosomal structural variants in all RELA tumors, which lead to the formation of neo-TADs placing the *REST Corepressor 2* (*RCOR2*) gene in a new regulatory environment (**Figure 2d, Suppl. Figure 2b**). *RCOR2* is located ~150kb away of *C11orf95* and has a strong enhancer element upstream of its transcription start site that forms new DNA interactions with the *C11orf95* gene and other nearby enhancer elements by bridging the *C11orf95-RELA* breakpoint (**Figure 2e, Suppl. Figure 2c**). By evaluating global Affymetrix gene expression array data[1] across ependymoma groups, we found that *RCOR2* expression is significantly upregulated in supratentorial RELA relative to other ependymoma groups (p-value=1.71e-91, **Figure 2f**) and is highly correlated with *C11orf95* transcription (R=0.66, p-value=6.93^{-11}, **Suppl. Figure 2d)**. Interestingly, we also identified RCOR2 as a hit in RELA cells in an independent shRNA screen (data not shown). To validate the relevance of RCOR2 for tumor growth and maintenance, we performed shRNA-mediated knock-down of *RCOR2* expression in patient derived RELA and PFA ependymoma cell lines. We observed that *RCOR2* knockdown results in strongly reduced cell survival of supratentorial RELA and to a lesser extent of PFA cell lines (**Figure 2g-h)**. The on-target effect of shRNAs against *RCOR2* was

confirmed by western blot analysis of RCOR2 protein in RELA ependymoma cells (**Suppl. Figure 2e**). RCOR2 can form a protein complex with the histone de-methylase LSD1, also known as KDM1A, and other transcriptional co-repressors, including HDAC1/2[22]. LSD1, HDAC1 and HDAC2 are all highly expressed across ependymoma subgroups and HDAC1/2 show pronounced RELA ependymoma-specific expression (**Suppl. Figures 2f-h**). Since there is no available compound against RCOR2, we reasoned that inhibition of other components of the RCOR2/LSD1/HDAC complex may still confer a therapeutic vulnerability for RELA ependymoma tumors. shRNA-mediated inhibition of *LSD1* expression indeed leads to a significant depletion of RELA but not PFA ependymoma cells compared to scrambled shRNA (**Figure 2i, Suppl. Figures 2i,j)**. Surprisingly, however, targeting the enzymatic activity of LSD1 with the LSD1 inhibitor ORY-1001[23] had no effect on cell survival using clinically accessible concentrations (**Figure 2j**), suggesting that in this protein complex the protein rather than the enzymatic activity of LSD1 is important. In contrast, targeting the HDAC activity in the complex with Entinostat, an HDAC1-3 inhibitor, strongly inhibited the survival of RELA ependymoma cells, while having less effect on PFA cells (**Figure 2k**). Combining ORY-1001 with Entinostat showed no synergy (data not shown) and also the results for Corin, a dual inhibitor of both LSD1 and HDACs, were not better than those for Entinostat alone (**Figure 2l**). Inhibition of other HDACs with, e.g., HDAC8 and HDAC6/10 inhibitors PCI-34051 and Tubastatin, respectively, had no effect on cell survival (**Suppl. Figure 2k-l**). Altogether, our data show that the CoREST protein complex containing RCOR2, LSD1 and HDAC1/2 has a crucial role in the growth and maintenance of supratentorial RELA ependymoma tumors that can be inhibited by disrupting the complex or by targeting the activity of HDACs.

PFA Ependymomas are dependent on integrin α6

In all PFA tumors the Hi-C data revealed a 3D chromatin cluster that spatially links numerous regulatory sequences and genes located more than 4 million base pairs apart on chromosome 2 (**Figure 3a-c, Suppl. Figure 3a**). To determine if this chromatin cluster is specific to PFA tumors, we analyzed Hi-C data obtained from RELA ependymoma samples as well as normal human tissues and cell types analyzed by the ENCODE and PsychENCODE consortia[24,25]. There was no sign of similar DNA interactions in the RELA and non-tumor samples, suggesting that this chromatin cluster is specific to PFA ependymomas (**Figure 3a, Suppl. Figure 3a**). By analyzing the expression of genes in this chromatin cluster in ependymoma and normal human brain samples, we observed that *integrin α6* (*ITGA6*) expression, encoding the receptor of the extracellular matrix protein laminin, is significantly upregulated in PFA compared to RELA ependymoma and also normal human brain tissues (p-value:

1.21e-114, **Suppl. Figure 3b**). As also reported previously[1], gene-ontology analysis shows that ITGA6-associated gene sets, such as *extracellular matrix organization* and *positive regulation of cell migration*, are among the most highly enriched biological processes when comparing overall gene expression profiles of PFA to other ependymoma groups (**Suppl. Table 5**). Recent genome-wide CRISPR-Cas9 inhibition screens have revealed that ITGA6 is highly and specifically essential in PFA ependymoma cell lines compared to glioblastoma (GBM) cell lines and fetal neural stem cells (fNSCs)[26,27] (**Suppl. Figure 3c**). In addition, we find that *integrin β4* (*ITGB4*), but not *β1* (*ITGB1*), is significantly up-regulated in PFA compared to RELA ependymoma and normal brain samples (p-values: 1.48e-119 and 1.42e-90, **Suppl. Figure 3d**), suggesting that the integrin α6β4 heterodimer is the functional form relevant for PFA tumors. Based on these results, we hypothesized that PFA ependymomas are locked in an oncogenic genomic topological configuration that activates *ITGA6* transcription and drives the acquisition and maintenance of stemness. To test this hypothesis, we performed CRISPR-Cas9 mediated *ITGA6* knock-out in patient-derived PFA ependymoma cells by cloning three different sgRNA sequences targeting *ITGA6* into a lentiviral vector expressing Cas9 in conjunction with GFP and subsequently transduced PFA ependymoma cells with the virus. As a result, we observe that transduced PFA ependymoma cells (**Figure 3d**), but neither transduced RELA ependymoma (**Suppl. Figure 3e**) nor glioblastoma cells (**Suppl. Figure 3f**), showed a gradual decrease in cell proliferation over time, validating *ITGA6* as an essential tumor-dependency gene specific for PFA ependymomas.

Transcriptional activation of LAMC1 as a potential resistance mechanism in recurrent PFA tumors

Conventional copy-number variation (CNV) analyses previously showed 1q copy-number gains in a subset of very aggressive and recurrent PFA ependymomas (**Suppl. Figure 3g**)[10]. By investigating CNVs in PFA tumors, including primary and relapse tumors of the same patient, we observed frequent increases in genomic instability in relapse tumors, while the 1q gain is maintained or emerges during tumor progression (**Suppl. Figure 3h**). To elucidate the molecular mechanisms associated with 1q gain, we systematically searched for SVs in all PFA ependymoma samples using the Hi-C data (**Suppl. Table 6**). As expected, primary PFA EPNs have frequent DNA interactions within chromosomes ('cis') and no DNA interactions indicative of recurrent structural variants **(Suppl. Figure 3i)**. However, we observed several complex inter-chromosomal DNA ('trans') interactions indicative of structural variants in PFA ependymoma relapse tumors **(Figure 3e, Suppl. Figure 3j)**. When comparing SVs among the analyzed PFA ependymoma relapse samples, we observed a recurring event that leads to an inversion of a ~66 Mb region of chromosome arm 1q into chromosome 8 (chr1-chr8

in sample EPD210FH, **Figure 3e**), or into chromosome 3 (chr1-chr3 in sample RD-19-157, **Suppl. Figure 3j**). In both cases, the breakpoints on chromosome 1q are located near the gene locus of *laminin subunit γ1* (*LAMC1*). Examination of the Hi-C data shows that both SVs led to the formation of neo-TADs, which place *LAMC1* into new regulatory environments **(Figure 3f,g)**. Inspecting RNA-seq expression data revealed that *LAMC1* is expressed almost three times higher in the two 1q+ PFA ependymoma relapse tumors than in primary PFA ependymoma tumors (**Figure 3h**). The same pattern of increased *LAMC1* expression in PFA relapse cases was found in a larger Affymetrix ependymoma data cohort[1] (**Figure 3i**). By a direct comparison of three relapse tumors that developed within 18 years after the primary diagnosis of a PFA ependymoma patient, we observed upregulation of *LAMC1* specifically in the third and fatal relapse tumor with marked chr1q gain (**Suppl. Figure 3h,k**). These results suggest that transcriptional activation of *LAMC1* by the formation of SV-induced neo-TADs is a resistance mechanism in recurrent 1q+ PFA EPN tumors that potentially promotes proliferation and stemness by further enhancing an already excessive integrin signaling. Based on these results, we hypothesized that *LAMC1* expression is essential for the proliferation and growth of PFA ependymoma tumors. To test this hypothesis, we performed genetic (CRISPR-Cas9) inhibition experiments against *LAMC1* and observed strongly reduced cell growth in the same PFA cell line EPD210FH that harbors the chr1-chr8 translocation (**Figure 3j, Suppl. Fig. 3l**) but not in RELA (**Suppl. Figure 3m**) ependymoma models.

Hypermethylation disrupts CTCF binding in PFA ependymoma

It has recently been shown that DNA methylation-mediated insulator dysfunction can lead to altered chromosomal topology thereby activating oncogenic programs (**Figure 4a**)[28,29]. Given the global loss of repressive H3K27me3[10,11] and a previously reported DNA methylation phenotype in PFA ependymoma[5], we hypothesized that similar molecular mechanisms may drive oncogene activation in this tumor type. Therefore, we analyzed 7 PFA (n=4) and RELA (n=3) tumors using Whole Genome Bisulfite Sequencing (WGBS) and CTCF ChIP-seq (**Suppl. Table 1**). As expected, genome wide CpG methylation is high in PFA and RELA ependymomas with low levels of methylation at functional regulatory elements, such as promoters, enhancers and insulators (**Suppl. Figure 4a**). By comparative analysis of DNA methylation at CTCF binding sites, we found that DNA hypermethylation replaces 2,387 CTCF binding sites in PFA tumors, but conversely is associated with the loss of only 178 CTCF binding sites in supratentorial RELA tumors (**Figure 4b-d**). The loss of CTCF binding through DNA hypermethylation is a predominant event in PFA ependymoma (**Figure 4c**) and can be associated with the formation of new enhancer-gene DNA loops and transcriptional activation of the target genes (**Suppl. Table 7**). To investigate whether such potential DNA methylation-mediated insulator

dysfunctions can be linked to the transcriptional activation of genes essential for PFA ependymoma, we compared our results with those of a genetic inhibition screen in PFA cell lines[26]. Among others, we observed localized hypermethylation in PFA tumors associated with the loss of a CTCF binding site and the formation of DNA interactions between non-coding regulatory enhancer elements and the *ADP Ribosylation Factor Like GTPase 4C* (*ARL4C*) gene (**Figure 4e-f**). *ARL4C* transcription is significantly (**p-value:** 4.25e-55) upregulated in PFA tumors compared to other ependymoma groups (**Suppl. Figure 4b**) and is highly correlated with the activity of the enhancer elements that physically interact with the *ARL4C* gene locus in PFA tumors (**Figure 4g, Suppl. Figure 4c**), but not in RELA tumors. It has been shown that ARL4C promotes migration, invasion and proliferation in colorectal and lung cancer[30] and recent genome-wide CRISPR-Cas9 inhibition screens revealed that ARL4C is essential for the proliferation of PFA ependymoma compared to glioblastoma cell lines (**Suppl. Figure 4d**)[26,27]. By genetic (CRISPR-Cas9) inhibition experiments we validated that ARL4C is highly and specifically essential for the growth of PFA ependymoma (**Figure 4h**) compared to RELA ependymoma and glioblastoma models (**Suppl. Figure 4e-f**). These results not only provide additional evidence for the relevance of ARL4C in PFA ependymoma tumors, but also shed light on the various molecular mechanisms that potentially lead to oncogenic activation of gene expression through genome-wide epigenetic alterations.

Discussion

By investigating 3D ependymoma genomes using Hi-C, we have identified multiple oncogenic chromatin conformations and novel tumor-dependency genes, pathways and potential therapeutic targets in RELA and PFA ependymoma. We show that structural variants in supratentorial tumors not only lead to *C11orf95-RELA* fusion genes, but also result in the formation of new regulatory environments that are recurrently associated with the aberrant overexpression of *RCOR2*. RCOR2 is the scaffold protein in the CoREST complex that further contains LSD1 and HDAC1 and HDAC2. The complex is associated with gene silencing and is known to play a role in cancer development[31]. Here, we have shown that both *RCOR2* and *LSD1* expression is essential in RELA ependymoma, but not or to a lesser extent in PFA ependymoma, and that the cells are sensitive to HDAC1/2 inhibitors in line with our previous observations[32]. However, inhibition of the enzymatic activity of LSD1 had no effect. These results suggest that the activities of HDAC1/2 may be critical in regulating CoREST repressor functions in RELA ependymoma. Recent work in small cell lung cancer (and Merkel cell carcinoma) also implicated that disrupting the CoREST complex, but not the inhibition of LSD1's enzymatic activities is required for blocking cancer cell proliferation[33]. Further studies identifying the

components of the CoREST complex and identifying drugs that can disrupt the complex will be instrumental in developing an effective CoREST-targeted therapy for RELA ependymoma.

Furthermore, we have shown that PFA ependymomas are not only characterized by diminished histone methylation and increased acetylation at histone 3 lysine 27 (H3K27), as recently reported[26], but also exhibit a tumor-specific 3D chromatin organization. Through targeting of *ITGA6*, a gene involved in a PFA-specific chromatin cluster, we demonstrate the importance of integrin signaling for maintained tumor growth, specifically in PFA tumors. ITGA6 has been described as a marker for cancer stem cells (CSCs) in several cancer types[34-38], where disruption of ITGA6 function suppresses the CSC phenotype and the maintenance of stem cells[34]. Our results provide evidence for an epigenetic dysregulation event that promotes integrin signaling and the acquisition of stemness in PFA ependymoma. The significance of integrin signaling for PFA tumor progression is further promoted by the recurrent transcriptional activation of *LAMC1* in PFA relapse tumors which frequently harbor gains of chromosome 1q. Although relapse tumors often show increased genomic instability, our Hi-C data showed for the first time an unexpected complexity of intra- and inter- chromosomal rearrangements underlying some chromosome-arm-wide copy number variations. Our results suggest that transcriptional activation of *LAMC1* by the formation of SV-induced neo-TADs is a potential resistance mechanism in recurrent 1q+ PFA EPN tumors that promotes proliferation and stemness by further enhancing already excessive integrin signaling. For other tumor types, LAMC1 has already been shown to be involved in tumor cell invasion and metastasis[39]. Thus, strategies that target integrin signaling, including ITGA6 and LAMC1, may reveal new vulnerabilities and overcome resistance to therapy in the treatment of PFA EPN relapse patients. Insulator dysfunction and oncogene activation by hypermethylation of CTCF binding sites has recently been described in IDH mutant gliomas and in SDH-deficient gastrointestinal stromal tumors (GISTs)[28,29]. Here, we show that PFA ependymoma is another tumor type with a global epigenetic phenotype in which there is hypermethylation of CTCF binding sites and associated changes in genome topology. By genetic inhibition of *ARL4C* in a PFA ependymoma model, we provide evidence that insulator dysfunction is a potential oncogenic mechanism in PFA ependymoma tumors and that tumor-dependency genes can be identified by 3D tumor genome profiling. Altogether, our study has identified several new group specific tumor dependencies in ependymoma, opening up avenues for potential novel therapeutic interventions that are highly needed in this disease, especially for RELA and PFA ependymoma. Our results will also be important for other (pediatric) cancers, especially those that relapse, where the drivers might be known, but where therapeutic options are scarce. Hi-C studies in these tumors may also reveal unknown tumor dependencies and new therapeutic targets.

Figures

Figure 1: 3D tumor genome profiling identifies PFA and RELA specific chromatin conformations and ependymoma enhancer associated genes.

(a) Overview of the major results obtained by the application of genome-wide chromosome conformation capture (Hi-C) in ependymoma brain tumors.

(b) Characteristics of ependymoma samples analyzed by Hi-C. One group of PFA ependymoma samples has no apparent copy-number variants, while the other group of PFA samples exhibits chromosome 1q gains associated with an unfavorable outcome.

(c) Unsupervised hierarchical clustering of PFA and RELA ependymoma tumors based on DNA interactions (Hi-C) stratifies the samples into the expected molecular groups.

(d) Integrative analysis of enhancers (H3K27ac ChIP-seq), chromosome conformation (Hi-C) and gene expression (RNA-seq) shows that genes are more strongly expressed when their promoters physically interact with other promoters or with enhancers. Shown are tumors (3x PF-A, 3x RELA) for which sample-matched H3K27ac ChIP-seq, RNA-seq, and HiC data are available. The center line, box limits and whiskers indicate the median, upper/lower quartiles and 1.5× interquartile range respectively. P-values from the bootstrap t-test are included.

(e) Re-evaluation of genes previously predicted to be regulated by PFA ependymoma enhancers confirms that the promoter regions of approximately 66% of these genes (n=1,028) physically interact with PFA ependymoma enhancers. Similar results (63%, n=1,229) are obtained for RELA ependymomas.

(f) The *TNC* promoter physically interacts with two distal enhancers (E1 and E2), whereby the interaction with the more proximal enhancer E1 is much more pronounced in PFA than in RELA tumors.

(g) *TNC* expression is positively correlated with the activity of the PFA-specific enhancer E1 (*chr9:118146925−118163777*), which is located 390kb upstream of the *TNC* transcription start site. Here, a cohort of 24 tumors from six different intracranial ependymoma groups was examined.

(h) The integrative analysis of Hi-C, enhancer and gene expression data reveals that more than twice as many genes as previously reported[18] are regulated by proximal and distal ependymoma enhancers.

(i) The Hi-C data identifies a cluster of DNA interactions between a RELA-specific superenhancer (SE) and the *EEF1A2* gene. This regulatory dependency was not recognized previously because Hi-C data obtained from IMR90 cells, which is commonly used as a reference, does not show any DNA interactions and topologically associated domains at the *EEF1A2* gene locus.

(j) *EEF1A2* expression is positively correlated with the RELA-specific SE (*chr20:62060923−62127745*) highlighted in panel i. This regulatory dependency is further supported by the many RELA-specific DNA interactions observed in the Hi-C data.

Figure 2: ***Transcriptional activation of RCOR2 by neo-TADs in RELA ependymoma***

(a) The Hi-C data reliably detect the structural variants that lead to the *C11orf95-RELA* fusion gene in supratentorial RELA-fusion associated tumors. Green boxes highlight SVs predicted by the computational methods applied.

(b) Chromothriptic rearrangements of chromosome 11 in a patient-derived RELA cell line (RELA BT165) visualized using Hi-C data.

(c) Structural variants in RELA tumors are not limited to chromosome 11 but also involve other chromosomes. Shown is an inter-chromosomal structural variant that includes chr11 and chr22 in tumor sample 7EP41.

(d) Reconstruction of the *C11orf95-RELA* breakpoint in a supratentorial tumor (4EP35) using Hi-C data reveals the formation of a neo-TAD that involves DNA interactions between *RCOR2* and the *C11orf95-RELA* fusion gene. RNA-seq and H3K27ac ChIP-seq data of this sample are included as additional tracks.

(e) Genome browser visualization of the *C11orf95* and *RCOR2* genomic region shows RELA ependymoma-specific enhancers and DNA interactions.

(f) Boxplot of *RCOR2* gene expression across ependymoma groups using Affymetrix gene expression data (n=393). The center line, box limits, whiskers and points indicate the median, upper/lower quartiles, 1.5× interquartile range and outliers, respectively. *RCOR2* is significantly upregulated in RELA tumors (anova p-val.: 1.71e-91).

(g-i) shRNA time-course knockdown experiments in RELA (EP1NS) and PFA (EPD210FH) ependymoma cell lines using a scrambled control and two shRNA constructs each targeting either *RCOR2* in EP1NS **(g),** *RCOR2* in EPD210FH **(h)** or *LSD1* in EP1NS **(i)**. All constructs are GFP tagged and GFP positive cells are sorted by FACS. Results are normalized to day 0 and error bars represent SEM from two independent experiments.

(j-l) Dose response curves of single-compound treatment with ORY-1001 **(j)**, Entinostat (**k**) or Corin **(l)** of RELA (EP1-NS) and PFA (EPD210FH) ependymoma spheroids over a 72-hour time-course using Celltiter-Glo cell viability assays. For each sample the results are presented as percentage of the Luminescence signal from control condition (i.e. water for ORY-1001 and DMSO for Entinostat and Corin as a vehicle). Data are presented as SEM from three independent experiments per tumor type.

Figure 3: PFA Ependymomas are dependent on integrin signaling

(a) Hi-C DNA interaction matrices wherein a ~5 million base pair segment of chromosome 2 is aligned along the diagonals shown for PFA (9EP1, left) and RELA (4EP53, middle) tumors and normal cerebellum astrocytes (CAs, right). Off-diagonal signals indicate DNA interactions between different genomic sites. The chromatin complex (highlighted by dashed circles) spatially links several genes, including *ITGA6*, and various regulatory elements located more than 4 million base pairs apart and is recurrently observed in all PFA ependymoma tumors, but in none of the other samples analyzed.

(b) Hi-C DNA interactions of a PFA tumor (sample BT214) wherein the same ~5 million base pair segment of chromosome 2 shown in panel (a) is aligned horizontally. Circles and dashed lines highlight long-range DNA interactions.

(c) Genome browser view of the PFA-specific chromatin cluster shown in panels (a) and (b). The included data tracks show long-range DNA interactions in PFA tumors ('Hi-C loops') as well as gene expression and H3K27ac in RELA and PFA tumors.

(d) Genetic (CRISPR-Cass9) time-course knockout of *ITGA6* in PFA ependymoma cells (EPD210FH) using an unspecific control and three individual sgRNA constructs. All constructs are GFP tagged and GFP positive cells are sorted by FACS. Results are normalized to day 0 and error bars represent SEM from two independent experiments.

(e) The conventional copy number profile of a PFA relapse sample (EPD210FH) shows high genomic instability including gain of chromosome arm 1q (presented vertically on the left). The genome-wide DNA interaction (Hi-C) map obtained from the same sample identifies complex inter-chromosomal structural variants including an inversion that involves chr1q and chr8. These trans-SVs reveal the complexity of genomic rearrangements underlying some copy-number gains and losses observed by common copy number variation analyses.

(f) Re-construction of the structural variant that involves chr1q and chr8 in the PFA relapse sample EPD210FH using Hi-C data. This structural variant results in the formation of a neo-TAD that places the *LAMC1* gene locus in a new regulatory environment.

(g) Re-construction of the structural variant that involves chr1q and chr3 in the PFA relapse tumor RD-19-157 using Hi-C data obtained from FFPE material. This structural variant also results in the formation of a neo-TAD that places the *LAMC1* gene locus in a new regulatory environment.

(h) Boxplot of RNA-seq expression analysis revealed that *LAMC1* is expressed almost three times higher in the two 1q+ PFA ependymoma relapse tumors than in primary PFA tumors, suggesting that the transcriptional activation of *LAMC1* by the formation of SV-induced neo-TADs is a common

resistance mechanism in recurrent 1q+ PFA EPN tumors. The center line, box limits, whiskers and circles indicate the median, upper/lower quartiles, 1.5× interquartile range and samples, respectively. **(i)** Boxplot of Affymetrix gene expression data shows that *LAMC1* tends to be upregulated in a larger cohort of relapse PFA in comparison to primary PFA ependymoma tumors. The center line, box limits, whiskers and points indicate the median, upper/lower quartiles, 1.5× interquartile range and outliers, respectively.
(j) Genetic (CRISPR-Cass9) time-course knockout of LAMC1 in PFA ependymoma cells (EPD210FH) using an unspecific control and three individual sgRNA constructs. All constructs are GFP tagged and GFP positive cells are sorted by FACS. Results are normalized to day 0 and error bars represent SEM from two independent experiments.

Figure 4. Hypermethylation replaces CTCF binding sites in PFA ependymoma.
(a) Proposed mechanism of epigenetic oncogene activation in PFA ependymoma tumors. Top: The oncogene is separated from an enhancer by a CTCF insulator, which forms a topological barrier. Below: The CTCF insulator is replaced by DNA methylation so that the enhancer can contact the oncogene and enhances its expression.
(b) The volcano plot shows significant differential CTCF binding sites between PFA and RELA ependymoma tumors (min *p-value*: 0.1). CTCF binding sites significantly hypermethylated in PFA relative to RELA tumors are marked in orange (min *q-value*: 0.05).
(c) Comparison of CTCF binding strength (CTCF ChIP-seq, x-axis, min *p-value* 0.1, min fold change: 0.5) and DNA methylation (WGBS, y-axis, min *q-value*: 0.05, min difference: 0.1) at CTCF binding sites that show significant differences between PFA and RELA ependymoma tumors.
(d) Heatmap of WGBS-derived DNA methylation at the 300 most significant CTCF binding sites lost in three PFA (left) and three RELA (right) ependymoma tumors. The heatmaps and the composite panels on top show that CTCF binding sites are commonly replaced by DNA methylation in PFA tumors.
(e) Genome browser visualization of PFA ependymoma-specific DNA loops that associate two PFA enhancers (E1 and E2) with the *ARL4C* gene locus located ~3,520 kbp away from the *ARL4C* transcription start site.
(f) WGBS-derived DNA methylation and CTCF ChIP-seq data from PFA and RELA ependymoma tumors show that a CTCF binding site separating the *ARLC4* gene from the E1 and E2 PFA enhancers is replaced by DNA methylation in PFA tumors.

(g) *ARL4C* gene expression is positively correlated with the activity of enhancer E2 (*chr2:237763494−237764993*) across a cohort of 24 ependymoma tumors form six different intracranial ependymoma groups.
(h) Genetic (CRISPR-Cass9) time-course knockout of *ARL4C* in PFA ependymoma cells (EPD210FH) using an unspecific control and three individual sgRNA constructs. All constructs are GFP tagged and GFP positive cells are sorted by FACS. Results are normalized to day 0 and error bars represent SEM from two independent experiments.

Supplementary Figure 1
(a) The number of DNA contacts obtained in the individual ependymoma samples as a quality measure for the Hi-C data.
(b) The tSNE dimensionality reduction visualization and unsupervised clustering of DNA methylation data from a cohort of ependymoma samples (n=1,182) separates PFA and RELA ependymomas into separate groups. The samples analyzed in this study by Hi-C are highlighted in red and orange. Blocks marked with an asterisk show a magnification of selected samples, for better visualization.
(c) Proportions of topologically associated domains (TADs) shared between ependymoma tumors. The comparison is performed among PFA (n=3) and RELA (n=3) ependymoma tumors that were also included in our previous enhancer-mapping study[18]. Hi-C data from two normal cerebellum astrocytes provided in the ENCODE database[40] were included as controls. The mean proportion of common TADs is 0.569 and the greatest similarity is found in TADs from samples of the same group (PFA, RELA and cerebellar astrocytes), while the common TAD proportions in the individual sample groups are smaller.
(d) Numbers of common TADs between EPN PFA (n=3) and RELA (n=3) samples from enhancer landscape study. The highest number of same TADs is among all samples.
(e) *TNC* expression is positively correlated across a cohort of 24 tumors from six different intracranial ependymoma groups with the activity of the PFA ependymoma-specific enhancer E2 (*chr9:118275447−118288653*) located upstream of the *TNC* transcription start site.
(f-g) Hi-C data visualization of a genomic region that includes the *EEF1A2* gene. The association between a RELA ependymoma super enhancer (SE) and the up regulation of *EEF1A2* transcription was not detected previously due to the lack of annotated TADs at this gene locus in the Hi-C data from IMR90 samples. TADs derived from IMR90 (blue), RELA (RELA BT, red), and PFA (EPD210FH, orange) ependymoma samples are visualized in boxes.

Supplementary Figure 2

(a) Visualization of the Hi-C data at the extended *C11orf95* and *RELA* gene locus in PFA ependymoma tumors shows the absence of structural variants.

(b) Reconstruction of the *C11orf95-RELA* breakpoint in RELA ependymoma tumors (7EP41 and 11EP22) using Hi-C data reveals the formation of a neo-TAD that involves DNA interactions between *RCOR2* and the *C11orf95-RELA* fusion gene. RNA-seq, CTCF and H3K27ac ChIP-seq data of these samples are included as additional tracks.

(c) Chr11 genome browser visualization showing DNA loops that span the *C11orf95* and *RELA* gene loci.

(d) Correlation between the expression of *RELA* and *RCOR2* (R=0.663, *p-val*=6.93e-11) in RELA ependymoma tumors (n=76) profiled by Affymetrix gene expression arrays.

(e) Knock-down of *RCOR2* expression in RELA ependymoma cells. Western blots show protein levels 4 days post infection with indicated shRNAs. B-actin is used as a loading control.

(f-h) Boxplots of *LSD1*, *HDAC1* and *HDAC2* gene expression across ependymoma subgroups using Affymetrix gene expression data (n=393, anova p-values: 9.77e-15, 1.02e-27, 1.20e-14). The center line, box limits, whiskers and points indicate the median, upper/lower quartiles, 1.5× interquartile range and outliers, respectively.

(i) Knock-down of *LSD1* expression in ependymoma cells. Western blots show protein levels 4 days post infection with indicated shRNAs. B-actin is used as a loading control.

(j) shRNA time-course knockdown experiments in a PFA ependymoma cell line (EPD210FH) using a scrambled control and two shRNA constructs targeting *LSD1*. All constructs are GFP tagged and GFP positive cells are sorted by FACS. Results are normalized to day 0 and error bars represent SEM from two independent experiments.

(k-l) Dose response curves of the HDAC8 inhibitor PCI-34051 **(k)** and the HDAC 6/10 inhibitor Tubastatin **(l)** treatment of RELA (EP1NS, red) and PFA (EPD210FH, orange) ependymoma spheroids over a 72-hour time-course using Celltiter-Glo cell viability assays. For each sample, the results are presented as percentage of the Luminescence signal from control condition (DMSO as a vehicle). Data are presented as SEM from three independent experiments per tumor type.

Supplementary Figure 3

(a) DNA interaction matrices derived from HiC data wherein a ~5 million base pair segment of chromosome 2 (172,407,031-177,907,030 bp) is aligned along the diagonals. Off-diagonal signals indicate DNA interactions between different genomic sites. The chromatin complex at the *ITGA6*

locus recurrently forms in all PFA EPN tumors analyzed (shown for samples 9EP1, 9EP9, and 7EP18 in the top row). This chromatin complex is not present in RELA ependymoma tumors (middle row). Moreover, normal human cell types analyzed by the ENCODE and PsychENCODE consortia, such as cerebellar astrocytes (CA), neural progenitor cells (NPCs) and embryonic fibroblasts (IMR90, bottom row), do not show signs of similar DNA interactions, suggesting that this chromatin complex is characteristic for PFA ependymoma tumors.

(b) Differential gene expression analysis of Affymetrix array data identified ITGA6 as significantly (FDR<0.01, two-sided Wilcoxon test) upregulated in PFA compared to RELA ependymoma tumors and normal brain samples (n=200 PFA, n=76 RELA, and n=225 normal human brain samples). In the boxplot the center line, box limits, whiskers and points indicate the median, upper/lower quartiles, 1.5× interquartile range and outliers, respectively.

(c) ITGA6 has been observed as an essential gene specifically in PFA ependymoma cell lines compared to glioblastoma stem cells (GSCs) and fetal neural stem cells (fNSCs) in a published CRISPR-Cas9 knock-out screen[26]. In the boxplot the center line, box limits and whiskers indicate the median, upper/lower quartiles and 1.5× interquartile range, respectively.

(d) Expression of two alternative ITGA6 heterodimer partner proteins ITGB1 and ITGB4. While *ITGB1* and *ITGB4* are highly expressed in PFA and RELA ependymoma tumors compared to normal brain samples, only *ITGB4* is significantly upregulated (FDR<0.01, two-sided Wilcoxon test) in PFA compared to RELA ependymoma tumors, suggesting that the integrin α6β4 heterodimer is the functional form relevant for PFA ependymoma tumors (n=200 PFA, n=76 RELA, and n=225 normal human brain samples). In the boxplots the center line, box limits, whiskers and points indicate the median, upper/lower quartiles, 1.5× interquartile range and outliers, respectively.

(e) Genetic (CRISPR-Cas9) time-course knockout of *ITGA6* in RELA ependymoma cells (EP1-NS) using an unspecific control and three individual sgRNA constructs. All constructs are GFP tagged and GFP positive cells are sorted by FACS. Results are normalized to day 0 and error bars represent SEM from two independent experiments.

(f) Genetic (CRISPR-Cas9) time-course knockout of *ITGA6* in glioblastoma (GBM2) cells using an unspecific control and three individual sgRNA constructs. All constructs are GFP tagged and GFP positive cells are sorted by FACS. Results are normalized to day 0 and error bars represent SEM from two independent experiments.

(g) Example of a copy number profile of a PFA ependymoma tumor (16EP7) harboring a 1q gain. The CNV profile was obtained from DNA methylation array data.

(h) Copy number profiles of a primary and three relapse PFA ependymoma tumors from the same patient (RD-19-157). The CNV profiles were obtained from DNA methylation array data.

(i) Visualization of Hi-C data obtained from a primary PFA ependymoma tumor (16EP7) harboring a 1q gain shows frequent DNA interactions within chromosomes but no DNA interactions indicative of inter-chromosomal structural variants.
(j) The conventional copy number profile of a PFA relapse sample (RD-19-157) shows high genomic instability including gain of chromosome arm 1q (presented vertically on the left). The genome-wide DNA interaction (Hi-C) map obtained from the same sample identifies complex inter-chromosomal structural variants including an inversion that involves chr1q and chr3.
(k) Expression of *LAMC1* in the three relapse tumors of patient RD-19-157 shows up-regulation of *LAMC1* in the third relapse tumor that harbors a 1q gain.
(l) Western blots show efficacy of sgRNAs targeting *LAMC1* and control sgRNA in EPD210FH cells. Mixture of different clones of infected EPD210FH cells are used to obtain protein extracts at day 5 post infection with indicated sgRNAs. B-actin is used as a loading control.
(m) Genetic (CRISPR-Cas9) time-course knockout of *LAMC1* in RELA ependymoma (EP1-NS) cells using an unspecific control and three individual sgRNA constructs. All constructs are GFP tagged and GFP positive cells are sorted by FACS. Results are normalized to day 0 and error bars represent SEM from two independent experiments.

Supplementary Figure 4

(a) Mean methylation of PFA and RELA ependymoma tumors at promoters, enhancers and CTCF binding sites. The center line, box limits, whiskers and points indicate the median, upper/lower quartiles, 1.5× interquartile range and outliers, respectively.
(b) Boxplot showing *ARL4C* gene expression across ependymoma subgroups (Affymetrix gene expression data for n=393 ependymoma tumors). The center line, box limits, whiskers and points indicate the median, upper/lower quartiles, 1.5× interquartile range and outliers, respectively. *ARL4C* is significantly upregulated in PFA compared to the other ependymoma types (anova p-val.: 4.25e-55).
(c) Positive correlation of *ARL4C* gene expression and the activity of enhancer E1 (*chr2:237545700−237546199*) across a cohort of 24 ependymoma tumors form six different intracranial ependymoma groups.
(d) *ARL4C* has been observed as an essential gene in PFA ependymoma cell lines in a published CRISPR-Cas9 knock-out screen[26]. In the boxplot the center line, box limits and whiskers indicate the median, upper/lower quartiles and 1.5× interquartile range, respectively.
(e) Genetic (CRISPR-Cas9) time-course knockout of *ARL4C* in RELA ependymoma (EP1-NS) cells using an unspecific control and three individual sgRNA constructs. All constructs are GFP tagged

and GFP positive cells are sorted by FACS. Results are normalized to day 0 and error bars represent SEM from two independent experiments.

(f) Genetic (CRISPR-Cas9) time-course knockout of *ARL4C* in glioblastoma (GBM2) cells using an unspecific control and three individual sgRNA constructs. All constructs are GFP tagged and GFP positive cells are sorted by FACS. Results are normalized to day 0 and error bars represent SEM from two independent experiments.

Supplementary Tables

Supplementary Table 1: Cohort of ependymoma tumor samples and available data types.

Supplementary Table 2: Enhancer associated genes supported by DNA loops in PFA ependymoma.

Supplementary Table 3: Enhancer associated genes supported by DNA loops in RELA ependymoma.

Supplementary Table 4: Structural variants in RELA ependymoma samples as identified by (a) hicBreakFinder. No additional filter was applied. (b) HiC SV/trans with adjusted filtering.

Supplementary Table 5: DAVID Gene Ontology analysis results for differentially expressed genes specific for PFA compared to other ependymoma subgroups.

Supplementary Table 6: Structural variants in PFA ependymoma samples as identified by (a) hicBreakFinder. No additional filter was applied. (b) HiC SV/trans with adjusted filtering.

Supplementary Table 7: Enhancer-associated genes supported by DNA loops that are potentially formed due to the replacement of CTCF binding sites by DNA methylation in PFA ependymoma tumors.

Supplementary Table 8: Overview of shRNA and sgRNA oligo sequences applied in experimental validation.

Supplementary Table 9: Drugs selected for experimental validation

Supplementary Table 10: Overview of antibodies applied in experimental validation.

Acknowledgements

We are thankful to David T. Jones for providing pediatric patient-derived SU-pcGBM2 cells. This work is supported by a Hannah's Heroes St. Baldrick's Scholar Award (LC) and funding from the NIH National Institute of Neurological Disorders and Stroke Institute R21 NS116455 (LC), the NIH National Cancer Institute U01 CA217885 (JPM), U01 CA184898 (JPM), U24 CA210004 (JPM and JTR); the NIH National Institute of General Medical Sciences R01GM074024 (JPM); and the NIH National Library of Medicine T15LM011271 for OC. The pediatric brain profiling at NYU in M.S. laboratory was in part supported by grants from the Friedberg Charitable Foundation and the Making Headway Foundation. Work in the laboratory of J.R.D. was supported by a NIH Early Independence Award (DP5 OD023071).

Contributions

K.O., A.C., M.K. and L.C. prepared the manuscript and figures. K.O., O.C., A.C., M.P. J.T.R., E.F.J. and A.S. performed data analysis and visualization. A.C., D.E.P., M.M., and J.M.H. performed experimental validations, N.G.C., M.L., D.M., S.N., and M.S. processed and analyzed tumor material, R.B., S.C., K.K., R.A.H. and D.R. generated Hi-C libraries from frozen and FFPE tumor material and cell lines, K.W.P., T.M., S.M., A.S., H.C., J.C., R.W.R., K.A.M., S.A.K., M.D.T., F.B., J.R., J.P.M., S.M.P., F.A. and J.R.D. contributed to the study design and data interpretation. L.C. designed the study and L.C. and M.K. co-supervised the project.

Methods

Chromosome conformation capture

Hi-C on frozen tumor tissue sample was carried out using protocols previously described for tissue Hi-C experiments[41]. In brief, frozen tissues are pulverized using a mortar and pestle kept cold on a bed of dry ice into a fine powder. The tissue powder was then transferred to a 15mL conical tube containing 5mLs of DPBS and fixed with 2% formaldehyde for 10 minutes. The fixation was quenched by addition of 0.2M Glycine. The fixed tissue was pelleted by centrifugation, washed 1x with DPBS, and then flash frozen until ready for further processing.

For Hi-C experiments, the fixed frozen tissue pellets were first resuspended in 3mLs of lysis buffer (10mM Tris-HCl pH 8.0, 5mM $CaCl_2$, 3mM MgAc, 2mM EDTA, 0.2mM EGTA, 1mM DTT, 0.1mM PMSF, 1X Complete Protease Inhibitors). The sample was transferred to an M-tube and dissociated using a GentleMACS Tissue dissociator (Miltenyi) using the "Protein M-tube" setting. The sample was removed from the M-tube into a 50mL conical. The M-tube was washed with 3mLs of lysis buffer with 0.4% Triton X-100 added, and this wash was combined with the original 3mLs of sample for a total volume of 6mLs with final concentration of 0.2% Triton X-100. The sample was then passed through a 40μM cell strainer. The strainer was washed with an additional 2mLs of lysis buffer with 0.2% Triton X-100. The sample was then centrifuged and washed with 1mL of lysis buffer with 0.2% Triton X-100. After centrifugation, the sample was resuspened in 0.5% SDS and processed with previously described *in situ* Hi-C method[42] using the MboI enzyme. Libraries were prepared using the Illumina TruSeq LT sequencing adaptors. Initial QC sequencing was first performed on a MiSeq to assess library quality, and if sufficient, was subject to production scale sequencing on the HiSeq X or NovaSeq platform, respectively.

Chromosome conformation capture from FFPE material

Hi-C experiments on FFPE material were carried out by Arima Genomics, Inc (San Diego, CA). Dewaxed and re-hydrated FFPE tissue was used as input to a modified version of the Arima-HiC Kit protocol. After the Arima-HiC protocol, Illumina-compatible sequencing libraries were prepared by shearing the proximally ligated DNA and then size-selecting DNA fragments using SPRI beads. The size-selected fragments containing ligation junctions were enriched using Enrichment Beads (provided in the Arima-HiC Kit), and converted into Illumina-compatible sequencing libraries using the Swift Accel-NGS 2S Plus kit (P/N: 21024) reagents. After adapter ligation, DNA was PCR amplified and

purified using SPRI beads. The purified DNA underwent standard QC (qPCR and Bioanalyzer) and sequenced on the NovaSeq following manufacturer's protocols.

Hi-C data processing

The sequencing reads alignment to hg19 human genome reference and chromatin contacts calling was performed using HiCPro 2.9.0 toolkit[43] allowing the bin sizes 5,10,50,100,250 and 500 Kbp. Main visualization and normalized full contacts extraction was performed with JuiceBox v0.7.5 toolkit[44] . Per sample loop calling was applied from FitHiC v2.0.6 method[45] on bin sizes 5 Kbp with maximum distance between bins 50 Mbp. TAD calling was performed based on 50 Kbp bins resolution using TopDom tool[46].

Unsupervised clustering of Hi-C data

Hi-C data processing produced interaction matrices in .juicebox format for 3 RELA and 8 PFA ependymoma tumors. For each tumor, unsupervised clustering features were computed using the *Eigenvector* utility from the Juicer Tools analysis toolkit.[47] Briefly, the Eigenvector utility computes A/B compartments as the first principal component of the Pearson correlation matrix of each intra-chromosomal contact matrix.[48] A/B compartments were computed using Knight-Ruiz normalization at 1Mb resolution. Unsupervised hierarchical clustering was performed on these features using Pearson correlation distance and average linkage, using the *heatmap.2* function from *gplots* R package.

Genes and enhancers connections via loops

The ChIP-seq derived enhancer signals along with genomic locations of group-specific enhancers and normalized RNA-seq gene expression profiles from epenymoma tumors cohort (n=25) were obtained from published materials of the corresponding study[18]. Genome was fragmented into 5 Kbp bins and output from FitHiC loop calling tool was used to find contacts between genes and enhancers. For this purpose the genes were assigned to bins based on the location of transcription start site (TSS, 2500 Kbp upstream and downstream of the gene stat loci), while enhancers based on the overlap. Loop boundary correspondence was assigned to gene and/or group-specific enhancer lying either within the bin or in the closest upstream/downstream bin. Enhancer associated gene was considered to be supported by loop if the TSS of it was lying in one loop anchor while enhancer in the other. Correlation analysis was performed based on the usage of updated InTAD package[49] v1.9.2.

Gene expression analysis

The global ependymoma tumor gene expression data integration was performed based on the usage of corresponding R2 platform materials with focus on Affymterix dataset from combined ependymoma tumors cohort with integration of normal brain tissues (n=618). Major of these ependymoma tumor Affymetrix materials were obtained from the corresponding main study[1] (GEO: GSE64415) with additional external inclusions (GEO: GSE50161, GSE50385, GSE21687, GSE3526). The gene ontology analysis was performed using DAVID tool[50] based on the usage of differentially expressed genes between PFA and other ependymoma groups achieved with R2 platform from the EPN global Affymetrix dataset. The RNA-sequencing materials from target EPN cohort samples were analyzed as previously described[18].

Structural variants (SV) discovery from Hi-C data

SV discovery from Hi-C data was performed using two independent toolkits. The first toolkit, hicBreakFinder (https://github.com/dixonlab/hic_breakfinder), was adjusted for the usage on hg19 human genome reference with taking into account additional filtering lists of false positives obtained from external cohorts[19]. Shortly, the tool scans for abrupt shifts in chromosomal connections in order to find possible outliers representing inter/intra-chromosomal events based on the selected threshold (t=0.6) and reports them in resolutions 1Mb, 100Kb and 10Kb. Final combined result contains the highest resolution for detected SV. The second toolkit, Hi-C structural variant discovery or HiCsv, consists of two parts and was adjusted for the usage of hg38 genome as the most up-to-date reference genome. First part of this toolkit, HiCtrans[21], focuses on inter-chromosomal translocations: it scans the inter-chromosomal contact matrices over multiple Hi-C resolutions for each possible pair of chromosomes from a given sample and predicts candidate SVs based on the changepoint analysis using binary segmentation. The intra-chromosomal translocations are also detected in this toolkit based on the dual pattern of off-diagonal enrichment and diagonal depletion of chromatin interactions in a Hi-C map across genomic regions. HiCsv detects enrichment of interactions through FitHiC2 algorithm[45] and uses an insulation score-based estimation (similar to TAD finding[51]) to identify depletion in interaction frequency. Finally, it applies a density-based clustering of enriched Hi-C interactions with high insulation scores to discover structural variants.

CTCF ChIP-sequencing

ChIP-sequencing procedure was prepared and performed as previously described[18]. Shortly, ChIP flash-frozen for ependymoma tumours was performed using 5 µg CTCF antibody per ChIP Active Motif. Enriched DNA was quantified and barcoded. Following library amplification, DNA fragments were sequenced using Illumina HiSeq 2000 100-bp paired-end sequencing.

766

767 **CTCF ChIP-seq data analysis**

768 Reads alignment was performed to hg19 reference with BWA v0.5.10[52]. Duplicate alignments were
769 removed using Picard (*http://broadinstitute.github.io/picard*). Peak calling was performed using Macs
770 v1.4[53]. Differential RELA peaks between EPN PFA and RELA were detected suing DiffBind R
771 package[54] with min adjusted p-value limit 0.05.

772

773 **Whole genome bisulfite sequencing (WGBS)**

774 WGBS procedure was prepared and performed as previously described[55]. Shortly, 5 µg of genomic
775 DNA were sheared using a Covaris device. After adaptor ligation, DNA fragments were isolated and
776 bisulphite converted using the EZ DNA Methylation kit (Zymo Research). PCR amplification of the
777 fragments was performed followed by library aliquots pooling. Sequencing was performed Illumina
778 HiSeq 2000 machine.

779

780 **WGBS data analysis**

781 Initial reads processing was performed using methylCtools v0.9.4 as previously described[55].
782 Differentially methylated regions were detected using metilene v0.2.6 tool[56] with min adjusted p-
783 value limit 0.05. Combined visualization of the methylation profiles within CTCF target regions was
784 performed using the EnrichedHeatmap R package. Search of target loops was performed based on the
785 presence of overlapping the DMRs with differential CTCF peaks within.

786

787 **Cell culture**

788 HEK293T cells (CRL-1273, American Type Culture Collection) were cultured as previously described
789 (citation). EPD210FH cells were grown in NeuroCult NS-A Basal Medium (STEMCELL
790 Technologies) supplemented with NeuroCult Proliferation Supplement (STEMCELL Technologies),
791 2mM L-glutamine 1% Penicillin/Streptomycin, 75ng/ml bovine serum albumin (BSA) and 20ng/ml of
792 EGF (Peprotech) and FGF-basic (Peprotech). EP1NS cells were grown in Neurobasalmedium A (Life
793 Technologies) supplemented with 1µg/ml of Heparin (Sigma), 2mM L-Glutamine and 20ng/ml of EGF
794 and FGF-basic. Cells were cultured as a neurospheres in tissue culture flasks. When they were cultured
795 as an adherent culture, flask was additionally coated with Laminin (L2020, Sigma) for EPD210FH
796 cells and with Geltrex (A1569601, Life Technologies) for EP1NS cells. Pediatric patient-derived SU-
797 pcGBM2 cells were cultivated as neurospheres as previously described. (Katrin Schramm paper,
798 2019). All cells were routinely tested free of mycoplasma contamination and authenticated by Single

Nucleotide Polymorphism profiling (Multiplexion GmbH). All cell models were grown at 37°C with 5% CO2.

Lentiviral Transduction

shRNA plasmids and sgRNA plasmids were constructed as previously described (STK3 paper). All oligos are ordered from Sigma. Target sequences of all oligos are listed in Supplementary Table S8. Transduction was performed in the presence of protamine sulfate (final concentration 5 ug/mL, Sigma-Aldrich) Transduced cells were further cultured and GFP signal was analyzed by BD FACS Canto for GFP expression. Reduction of the percentage of GFP-positive cells indicates that the infected cells expressing a particular shRNA/ sgRNA have a growth disadvantage in comparison to the non-infected cells.

Drug treatments

All drugs were prepared according to protocols provided by company (Supplementary Table S9) Cells were seeded into 96-well cell culture treated plates at a density of 5000 cells in 100 µl respected medium per well. On the next day morning, cells were treated with increasing concentrations (200 nM, 400 nM, 800 nM, 1.6 µM, 3.2 µM, 6.4 µM and 12.8 µM) of each drug or equivalent dilutions of solvent. Cell viability was assessed after 72 hours using the CellTiter-Glo® luminescent cell viability assay (Promega) and an automated plate reader Mythras. All samples were assayed in triplicates and normalized to the average values of the corresponding mock control on the same plate and analyzed using Prism 8 (GraphPad).

Western blot analysis

For knockdown and/or knockout studies, cells were infected as described above and cultured for either 4 days (knockdown) or 5 days (knockout). Before harvesting, cells were washed with phosphate buffered saline (PBS) and collected as pellets. Then, pellets were lysed in RIPA buffer (Sigma-Aldrich) supplemented with protease and phosphatase inhibitors for 30 minutes on ice. After centrifugation at 13,000 rpm for 10 minutes at 4 °C, the supernatants were collected and protein concentrations were determined using a Bicinchoninic acid (BCA) assay (Sigma-Aldrich) with PierceTM bovine serum albumin standards (Thermo Fisher). Lysates were mixed with NuPAGE® LSD Sample buffer (Life Technologies) supplemented with 10 % 2-mercaptoethanol and denatured for 5 minutes at 95 °C. Afterwards they were subjected to sodium dodecyl sulfate-polyacrylamide gel electrophoresis according to standard procedures using 4-12 % Bis-Tris gels and afterwards transferred to polyvinylidene difluoride membranes. Membranes were incubated with respective primary

antibodies at 4 °C overnight (Supplementary Table S10). Horseradish peroxidase-conjugated anti-rabbit (1:5,000, Santa Cruz, sc-2054) secondary antibody were applied for 1 hour at room temperature and chemiluminescent detection was carried out using AmershamTM ECLTM or ECLTM Prime Western Blotting detection reagents (GE Healthcare). The same membranes were stripped with stripping buffer (Sigma) according to protocol and incubated with conjugated beta-actin antibody as a loading control.

Data availability

The novel sequencing data raw materials (HiC, CTCF, WGBS) will be included into the European Genome-phenome archive (https://www.ebi.ac.uk/ega/home) under the accession number: GAS00001002696; this source already contains other data types (RNA-seq, H3K27ac) for the corresponding target tumor samples.

Code availability

Scripts for processing the raw data and generating figures can be obtained upon request.

References

1 Pajtler, K. W. *et al.* Molecular Classification of Ependymal Tumors across All CNS Compartments, Histopathological Grades, and Age Groups. *Cancer Cell* **27**, 728-743, doi:10.1016/j.ccell.2015.04.002 (2015).

2 Pui, C. H., Gajjar, A. J., Kane, J. R., Qaddoumi, I. A. & Pappo, A. S. Challenging issues in pediatric oncology. *Nat Rev Clin Oncol* **8**, 540-549, doi:10.1038/nrclinonc.2011.95 (2011).

3 Siegel, R. L., Miller, K. D. & Jemal, A. Cancer statistics, 2016. *CA Cancer J Clin* **66**, 7-30, doi:10.3322/caac.21332 (2016).

4 Downing, J. R. *et al.* The Pediatric Cancer Genome Project. *Nat Genet* **44**, 619-622, doi:10.1038/ng.2287 (2012).

5 Mack, S. C. *et al.* Epigenomic alterations define lethal CIMP-positive ependymomas of infancy. *Nature* **506**, 445-450, doi:10.1038/nature13108 (2014).

6 Witt, H. *et al.* Delineation of two clinically and molecularly distinct subgroups of posterior fossa ependymoma. *Cancer Cell* **20**, 143-157, doi:10.1016/j.ccr.2011.07.007 (2011).

7 Parker, M. *et al.* C11orf95-RELA fusions drive oncogenic NF-kappaB signalling in ependymoma. *Nature* **506**, 451-455, doi:10.1038/nature13109 (2014).

8 Pajtler, K. W. *et al.* YAP1 subgroup supratentorial ependymoma requires TEAD and nuclear factor I-mediated transcriptional programmes for tumorigenesis. *Nature communications* **10**, 1-16 (2019).

9 Panwalkar, P. *et al.* Immunohistochemical analysis of H3K27me3 demonstrates global reduction in group-A childhood posterior fossa ependymoma and is a powerful predictor of outcome. *Acta Neuropathol* **134**, 705-714, doi:10.1007/s00401-017-1752-4 (2017).

10 Pajtler, K. W. *et al.* Molecular heterogeneity and CXorf67 alterations in posterior fossa group A (PFA) ependymomas. *Acta Neuropathol* **136**, 211-226, doi:10.1007/s00401-018-1877-0 (2018).

11 Hubner, J. M. *et al.* EZHIP / CXorf67 mimics K27M mutated oncohistones and functions as an intrinsic inhibitor of PRC2 function in aggressive posterior fossa ependymoma. *Neuro Oncol*, doi:10.1093/neuonc/noz058 (2019).

12 Araki, A. *et al.* Chromosome 1q gain and tenascin-C expression are candidate markers to define different risk groups in pediatric posterior fossa ependymoma. *Acta neuropathologica communications* **4**, 88 (2016).

13 Grubert, F. *et al.* Landscape of cohesin-mediated chromatin loops in the human genome. *Nature* **583**, 737-743 (2020).

14 Rhie, S. K. *et al.* A high-resolution 3D epigenomic map reveals insights into the creation of the prostate cancer transcriptome. *Nature communications* **10**, 1-12 (2019).

15 Kloetgen, A. *et al.* Three-dimensional chromatin landscapes in T cell acute lymphoblastic leukemia. *Nature Genetics* **52**, 388-400 (2020).

16 Li, Y., Hu, M. & Shen, Y. Gene regulation in the 3D genome. *Hum Mol Genet* **27**, R228-R233, doi:10.1093/hmg/ddy164 (2018).

17 Capper, D. *et al.* DNA methylation-based classification of central nervous system tumours. *Nature* **555**, 469-474 (2018).

18 Mack, S. C. *et al.* Therapeutic targeting of ependymoma as informed by oncogenic enhancer profiling. *Nature* **553**, 101-105, doi:10.1038/nature25169 (2018).

19 Dixon, J. R. *et al.* Integrative detection and analysis of structural variation in cancer genomes. *Nat Genet* **50**, 1388-1398, doi:10.1038/s41588-018-0195-8 (2018).

20 Lupianez, D. G. *et al.* Disruptions of topological chromatin domains cause pathogenic rewiring of gene-enhancer interactions. *Cell* **161**, 1012-1025, doi:10.1016/j.cell.2015.04.004 (2015).

21 Chakraborty, A. & Ay, F. Identification of copy number variations and translocations in cancer cells from Hi-C data. *Bioinformatics* **34**, 338-345 (2018).

22 Wang, Y. *et al.* LSD1 co-repressor Rcor2 orchestrates neurogenesis in the developing mouse brain. *Nature communications* **7**, 10481, doi:10.1038/ncomms10481 (2016).
23 Maes, T. *et al.* ORY-1001, a potent and selective covalent KDM1A inhibitor, for the treatment of acute leukemia. *Cancer Cell* **33**, 495-511. e412 (2018).
24 Rajarajan, P. *et al.* Neuron-specific signatures in the chromosomal connectome associated with schizophrenia risk. *Science (New York, N.Y.)* **362**, doi:10.1126/science.aat4311 (2018).
25 Davis, C. A. *et al.* The Encyclopedia of DNA elements (ENCODE): data portal update. *Nucleic acids research* **46**, D794-D801, doi:10.1093/nar/gkx1081 (2018).
26 Michealraj, K. A. *et al.* Metabolic Regulation of the Epigenome Drives Lethal Infantile Ependymoma. *Cell*, doi:10.1016/j.cell.2020.04.047 (2020).
27 MacLeod, G. *et al.* Genome-Wide CRISPR-Cas9 Screens Expose Genetic Vulnerabilities and Mechanisms of Temozolomide Sensitivity in Glioblastoma Stem Cells. *Cell Rep* **27**, 971-986 e979, doi:10.1016/j.celrep.2019.03.047 (2019).
28 Flavahan, W. A. *et al.* Insulator dysfunction and oncogene activation in IDH mutant gliomas. *Nature* **529**, 110-114, doi:10.1038/nature16490 (2016).
29 Flavahan, W. A. *et al.* Altered chromosomal topology drives oncogenic programs in SDH-deficient GISTs. *Nature* **575**, 229-233, doi:10.1038/s41586-019-1668-3 (2019).
30 Fujii, S., Matsumoto, S., Nojima, S., Morii, E. & Kikuchi, A. Arl4c expression in colorectal and lung cancers promotes tumorigenesis and may represent a novel therapeutic target. *Oncogene* **34**, 4834-4844, doi:10.1038/onc.2014.402 (2015).
31 Takagi, S. *et al.* LSD1 inhibitor T-3775440 inhibits SCLC cell proliferation by disrupting LSD1 interactions with SNAG domain proteins INSM1 and GFI1B. *Cancer Research* **77**, 4652-4662 (2017).
32 Milde, T. *et al.* A novel human high-risk ependymoma stem cell model reveals the differentiation-inducing potential of the histone deacetylase inhibitor Vorinostat. *Acta neuropathologica* **122**, 637 (2011).
33 Park, D. E. *et al.* Merkel cell polyomavirus activates LSD1-mediated blockade of non-canonical BAF to regulate transformation and tumorigenesis. *Nature Cell Biology* **22**, 603-615 (2020).
34 Lathia, J. D. *et al.* Integrin alpha 6 regulates glioblastoma stem cells. *Cell Stem Cell* **6**, 421-432, doi:10.1016/j.stem.2010.02.018 (2010).
35 Martin, T. A. & Jiang, W. G. Evaluation of the expression of stem cell markers in human breast cancer reveals a correlation with clinical progression and metastatic disease in ductal carcinoma. *Oncol Rep* **31**, 262-272, doi:10.3892/or.2013.2813 (2014).

36 Hoogland, A. M. *et al.* Validation of stem cell markers in clinical prostate cancer: alpha6-integrin is predictive for non-aggressive disease. *Prostate* **74**, 488-496, doi:10.1002/pros.22768 (2014).

37 Schober, M. & Fuchs, E. Tumor-initiating stem cells of squamous cell carcinomas and their control by TGF-beta and integrin/focal adhesion kinase (FAK) signaling. *Proceedings of the National Academy of Sciences of the United States of America* **108**, 10544-10549, doi:10.1073/pnas.1107807108 (2011).

38 Haraguchi, N. *et al.* CD49f-positive cell population efficiently enriches colon cancer-initiating cells. *Int J Oncol* **43**, 425-430, doi:10.3892/ijo.2013.1955 (2013).

39 Zhang, Y. *et al.* Overexpression of LAMC1 predicts poor prognosis and enhances tumor cell invasion and migration in hepatocellular carcinoma. *J Cancer* **8**, 2992-3000, doi:10.7150/jca.21038 (2017).

40 Consortium, E. P. An integrated encyclopedia of DNA elements in the human genome. *Nature* **489**, 57-74 (2012).

41 Schmitt, A. D. *et al.* A compendium of chromatin contact maps reveals spatially active regions in the human genome. *Cell reports* **17**, 2042-2059 (2016).

42 Rao, S. S. *et al.* A 3D map of the human genome at kilobase resolution reveals principles of chromatin looping. *Cell* **159**, 1665-1680 (2014).

43 Servant, N. *et al.* HiC-Pro: an optimized and flexible pipeline for Hi-C data processing. *Genome biology* **16**, 259 (2015).

44 Durand, N. C. *et al.* Juicebox provides a visualization system for Hi-C contact maps with unlimited zoom. *Cell systems* **3**, 99-101 (2016).

45 Kaul, A., Bhattacharyya, S. & Ay, F. Identifying statistically significant chromatin contacts from Hi-C data with FitHiC2. *Nature Protocols* **15**, 991-1012 (2020).

46 Shin, H. *et al.* TopDom: an efficient and deterministic method for identifying topological domains in genomes. *Nucleic acids research* **44**, e70-e70 (2016).

47 Durand, N. C. *et al.* Juicer Provides a One-Click System for Analyzing Loop-Resolution Hi-C Experiments. *Cell systems* **3**, 95-98, doi:10.1016/j.cels.2016.07.002 (2016).

48 Lieberman-Aiden, E. *et al.* Comprehensive mapping of long-range interactions reveals folding principles of the human genome. *Science (New York, N.Y.)* **326**, 289-293, doi:10.1126/science.1181369 (2009).

49 Okonechnikov, K., Erkek, S., Korbel, J. O., Pfister, S. M. & Chavez, L. InTAD: chromosome conformation guided analysis of enhancer target genes. *BMC bioinformatics* **20**, 60 (2019).

50 Sherman, B. T. & Lempicki, R. A. Systematic and integrative analysis of large gene lists using DAVID bioinformatics resources. *Nature protocols* **4**, 44 (2009).
51 Dixon, J. R. *et al.* Topological domains in mammalian genomes identified by analysis of chromatin interactions. *Nature* **485**, 376-380 (2012).
52 Li, H. & Durbin, R. Fast and accurate short read alignment with Burrows–Wheeler transform. *bioinformatics* **25**, 1754-1760 (2009).
53 Zhang, Y. *et al.* Model-based analysis of ChIP-Seq (MACS). *Genome biology* **9**, 1-9 (2008).
54 Ross-Innes, C. S. *et al.* Differential oestrogen receptor binding is associated with clinical outcome in breast cancer. *Nature* **481**, 389-393 (2012).
55 Hovestadt, V. *et al.* Decoding the regulatory landscape of medulloblastoma using DNA methylation sequencing. *Nature* **510**, 537-541 (2014).
56 Jühling, F. *et al.* metilene: Fast and sensitive calling of differentially methylated regions from bisulfite sequencing data. *Genome research* **26**, 256-262 (2016).

Figures

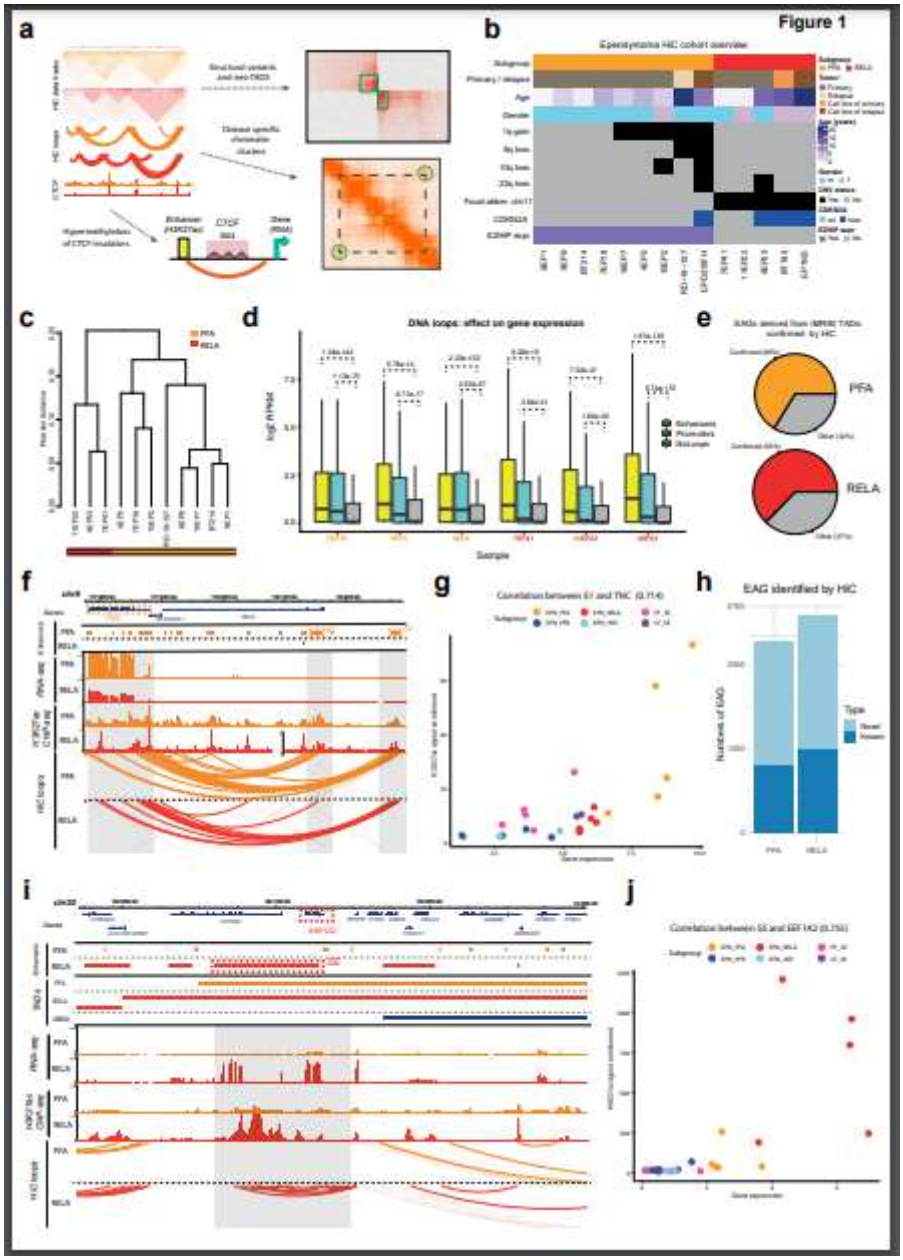

Figure 1

[Please see the manuscript file to view the figure caption.]

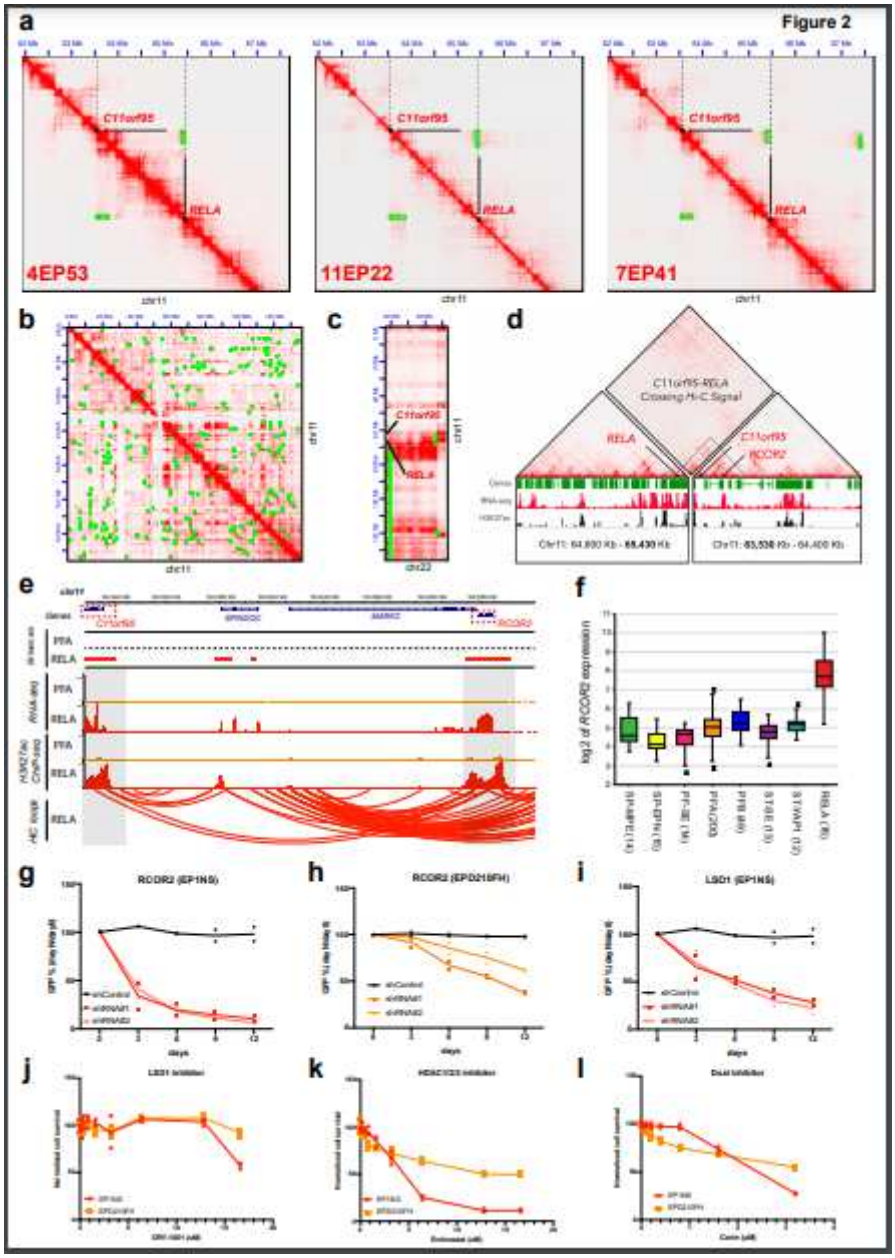

Figure 2

[Please see the manuscript file to view the figure caption.]

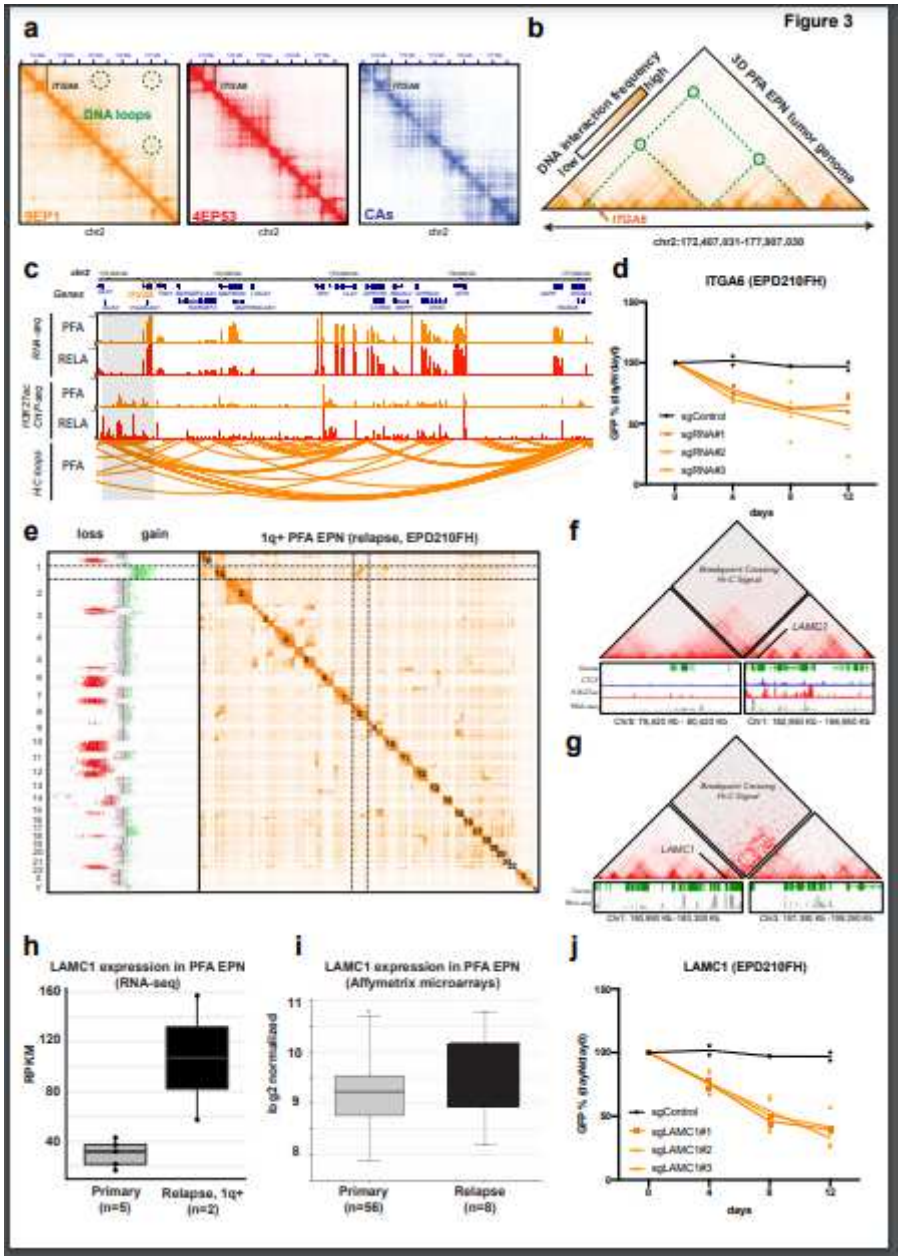

Figure 3

[Please see the manuscript file to view the figure caption.]

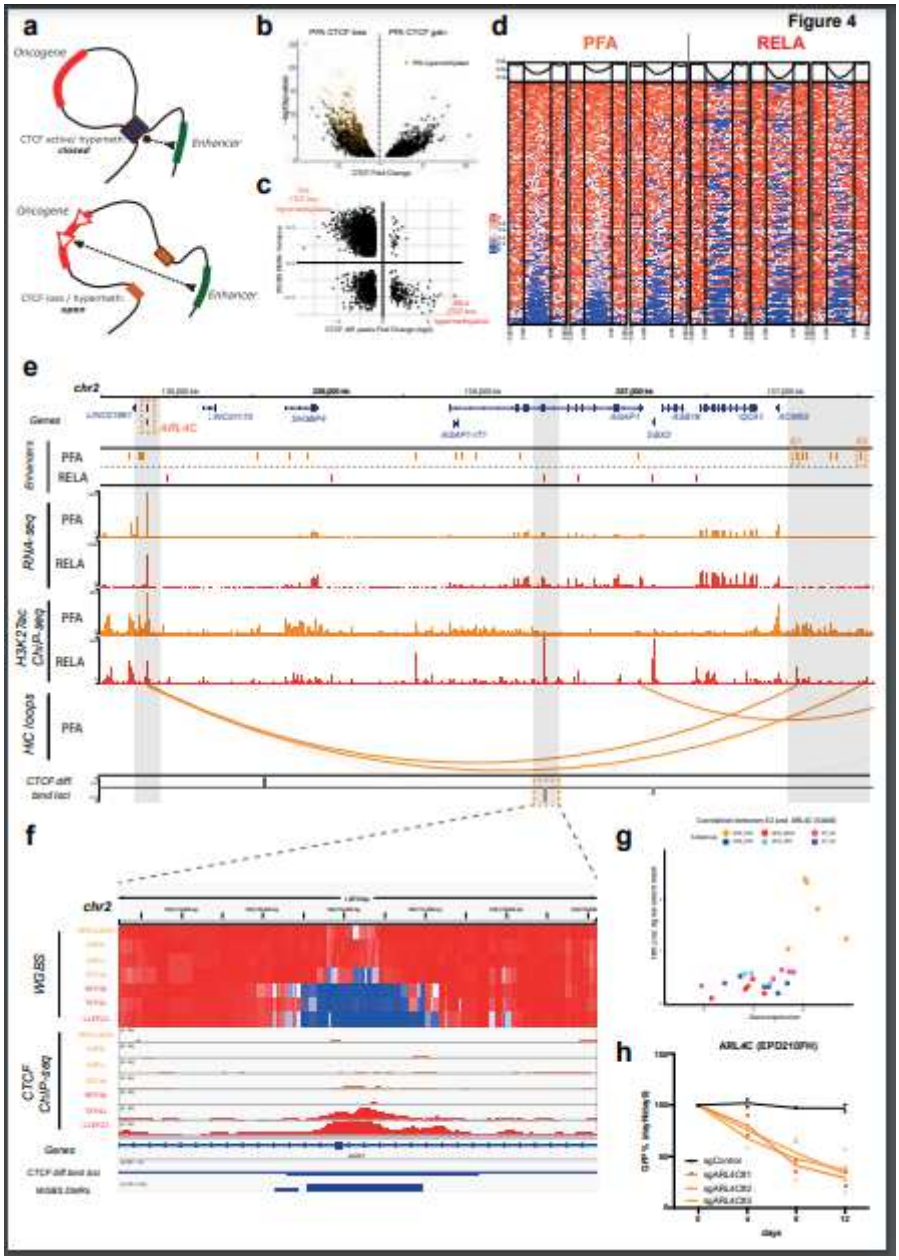

Figure 4

[Please see the manuscript file to view the figure caption.]

Supplementary Files

This is a list of supplementary files associated with this preprint. Click to download.

- EPNHiCtables.011020.xlsx
- SuppFigure1041020.pdf
- SuppFigure2041020.pdf
- SuppFigure3041020.pdf
- SuppFigure4041020.pdf